Nanoscale

# Haloperoxidase-Mimicking CeO2-x Nanorods for the Deactivation of Human Coronavirus OC43

| | |
|---|---|
| Journal: | *Nanoscale* |
| Manuscript ID | NR-COM-10-2021-006966.R1 |
| Article Type: | Communication |
| Date Submitted by the Author: | 13-Feb-2022 |
| Complete List of Authors: | Lang, Jiayan; Cornell University, Chemical and Biomolecular Engineering<br>Ma, Xiaojing; Cornell University, Chemical and Biomolecular Engineering<br>Chen, Pengyu; Cornell University, Chemical and Biomolecular Engineering<br>Serota, Max; Cornell University, Chemical and Biomolecular Engineering<br>Andre, Nicole; Cornell University, College of Veterinary Medicine<br>Whittaker, Gary; Cornell University, College of Veterinary Medicine<br>Yang, Rong; Cornell University, Chemical and Biomolecular Engineering |
| | |

SCHOLARONE™
Manuscripts

Please do not adjust margins

COMMUNICATION

# Haloperoxidase-Mimicking $CeO_{2-x}$ nanorods for the Deactivation of Human Coronavirus OC43

Received 00th January 20xx,
Accepted 00th January 20xx

DOI: 10.1039/x0xx00000x

Jiayan Lang,[a] Xiaojing Ma,[a] Pengyu Chen,[a] Max D. Serota,[a] Nicole M. Andre,[b] Gary R. Whittaker,[b] Rong Yang*[a]

**Abstract: Despite the excellent antibacterial and antifouling effects of haloperoxidase (HPO)-mimicking $CeO_{2-x}$ nanorods, their antiviral efficiency has not been explored. Herein, we designed and synthesized $CeO_{2-x}$ nanorods with varying aspect ratios via the hydrothermal method. $CeO_{2-x}$ nanorods catalysed the oxidative bromination of $Br^-$ and $H_2O_2$ to HOBr, the kinetics of which were studied systematically using a phenol red assay. The $CeO_{2-x}$ nanorods with the optimized aspect ratio (i.e., 4.5) demonstrated strong antiviral efficacies against the human coronavirus OC43, with no visible toxicity to the HCT-8 host cells.**

Viruses are responsible for the greatest global mortality from infectious diseases in the past ten years,[1, 2] with notorious examples ranging from the coronaviruses SARS-CoV and SARS-CoV-2, to Ebola virus and HIV/AIDs.[3] Unfortunately, the variety of available options for antiviral treatment remains limited.[4] The current best practice to mitigate viral infections is vaccination;[5] however, not all viruses have effective vaccines and many diseases with effective vaccines still require additional countermeasures-based on vaccine hesitancy and distribution challenges, and waning protection based on immunological durability or "immune-escape" viral variants.[6] Thus, antiviral and virucidal approaches remain important.

Hypohalous acid (HOX), such as hypochlorous acid (HOCl) is a strong oxidizing agent that could denature proteins and lead to formation of protein aggregations.[7, 8] Furthermore, HOCl has been reported to deactivate viruses via chlorination, i.e., by forming chloramines and nitrogen-centered radicals that break down the single- and double-stranded DNA.[7] Nevertheless, HOX has not been broadly applied as an virucidal due to its short half-life and cumbersome synthesis approaches that are predominantly based on electrolysis.[9] Alternatively, HOX could be synthesized via haloperoxidase (HPO) or HPO-mimicking reaction systems.[10] HPO-based virucidal mechanism is promising for virus inactivation since reported by Ray et al. at 1970.[11] HPO catalyzes the oxidation of halides $X^-$ ($Cl^-$, $Br^-$, $I^-$) to their corresponding HOX using hydrogen peroxide ($H_2O_2$) as the oxidant.[10] Using that mechanism, HOX, such as HOCl and hypobromous acid (HOBr) are produced endogenously in mammalian cells (e.g., those produced by myeloperoxidase in neutrophils)[12] and thus simultaneously possess excellent biocompatibility and broad-spectrum antimicrobial efficacy.[13]

Catalytic nanoparticles with enzyme-like activities, namely nanozymes,[14, 15] have demonstrated excellent stability, high catalytic efficiency, and low cost compared with their biological counterparts.[16] Cerium oxide ($CeO_{2-x}$) nanoparticles (also known as nanoceria) have been reported to have superoxide dismutase (SOD)-,[17] catalase (CAT)-,[18, 19] peroxidase-[20] and HPO-like[21, 22] activities. The SOD- and CAT-like activities have recently been reported to render $CeO_{2-x}$ nanoparticles scavengers for reactive oxygen species (ROS), thus providing protection to mammalian cells against oxidative damages.[23, 24]

The HPO-like activity makes $CeO_{2-x}$ nanorods a promising candidate for antiviral applications. The HPO-like properties of $CeO_{2-x}$ nanorods have been attributed to the facile redox cycle enabled by the $Ce^{3+}/Ce^{4+}$ states, via the reaction: $CeO_2 \leftrightarrow \square CeO_{2-x} + x/2O_2$.[21] Nevertheless, despite the extensive studies on the antifouling,[21] antibacterial,[25] and antioxidant[17] properties of $CeO_{2-x}$ nanorods, their antiviral properties remained unknown.

[a] Robert F. Smith School of Chemical & Biomolecular Engineering, Cornell University, Ithaca, NY 14853
[b] Dept. Microbiology & Immunology and Public Health Program, Cornell University, Ithaca, NY 14853

Electronic Supplementary Information (ESI) available: [details of any supplementary information available should be included here]. See DOI: 10.1039/x0xx00000x

Please do not adjust margins

Herein, $CeO_{2-x}$ nanorods with different lengths and aspect ratios were synthesized by systematically varying the concentration of

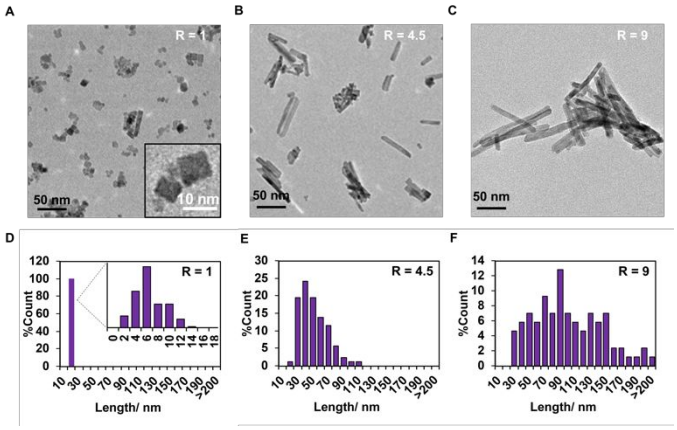


**Fig.1. TEM analysis of the $CeO_{2-x}$ nanorods with different R ratios**. (A-C) TEM images of $CeO_{2-x}$ nanorods with R ratios of A) R=1, B) R=4.5; and C) R=9. (D-F) Distributions of the lengths of the $CeO_{2-x}$ nanorods based on the TEM images.

sodium hydroxide (NaOH) during the hydrothermal synthesis process. The $CeO_{2-x}$ nanorods with the greatest catalytic activities also demonstrated the strongest virucidal efficacy against human coronavirus, HCoV-OC43, with no discernable toxicity to the host cells (i.e., human ileocecal adenocarcinoma HCT-8 cell line). This study provided a new design strategy for antiviral materials, one that leveraged the enzyme-mimicking catalytic activities of inorganic nanomaterials to generate antiseptics in situ for strong antiviral efficacies.

$CeO_{2-x}$ nanorods with different lengths and aspect ratios were synthesized via an established hydrothermal method.[21, 25] The hydrothermal approach leverages the dissolution and recrystallization of $CeO_{2-x}$ to control the growth of the nanoparticles,[26] where dissolved hydroxide ions promote the nucleation of cerium hydroxide. As such, lengths of the nanorods were varied by tuning the concentration of NaOH to be 1M, 5M, and 9M, and subsequently confirmed using transmission electron microscopy (TEM) (Fig. 1, Fig. S1, and Table S1).

While the as-synthesized nanoparticles demonstrated a uniform width of ~10 nm, the distribution of their length could be broad (Fig. 1C-F), which we quantified by analyzing non-overlapping TEM images of 150 nanorods and measuring their length using ImageJ. The NaOH concentration of 1M gave rise to the cubic $CeO_{2-x}$ nanoparticle with a diameter of 11.2 ± 4.7 nm and a length of 7.5 ± 2.5 nm, corresponding to an average aspect ratio (R) of ~1 (Fig. 1A). The length distribution was relatively uniform, following a pseudo-Gaussian form (Fig. 1D). Increasing the NaOH concentration to 5M led to increased length of the $CeO_{2-x}$ nanorods to 46.0 ± 17.9 nm, while the diameter remained unchanged (i.e., 11.9 ± 4.0 nm), corresponding to an average aspect ratio of ~4.5 (Fig. 1B). The length distribution became broader, while transitioning a Fisher–Snedecor form (Fig. 1E), implying that two independent growth processes might be at play (e.g., nucleation and anisotropic growth). Further increasing the NaOH concentration to 9M led to the greatest particle length, i.e., 86.9 ± 40.1 nm, with diameter of ~12.0 ± 2.5 nm and an average aspect ratio of ~9 (Fig. 1C). The length

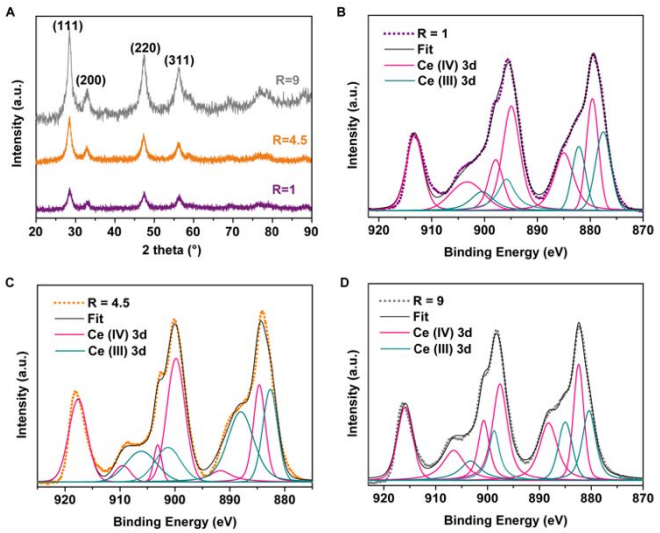


**Fig. 2.** (A) XRD patterns of the $CeO_{2-x}$ nanorods. (B-D) XPS high-resolution scan of Ce(3d) in the $CeO_{2-x}$ nanorods with R ratios of B) R=1, C) R=4.5; and C) R=9, and the peak deconvolution results. Dots indicate raw data; black solid lines correspond to the fitted curves based on peak deconvolution.

distribution was the broadest for these nanorods (Fig. 1F), which seemingly transitioned back to a pseudo-Gaussian distribution, hinting that the growth was dominated by a mechanism (likely the anisotropic growth step). Overall, higher concentration of NaOH led to formation of $CeO_{2-x}$ nanorods with higher aspect ratios, as the $CeO_{2-x}$ nuclei to grow anisotropically to form nanorods. The low rate of crystallization at the NaOH concentration of 1M led to slow growth of the $CeO_{2-x}$ nanorods, which resembled nanocubes by the end of the synthesis. All there three nanorods have negative surface that around -14 mV (Table S1).

To shed light on the internal structures of the $CeO_{2-x}$ nanorods, X-ray powder diffraction (XRD) patterns were collected and analyzed in combination with the TEM images (Figure 1). The XRD pattern of the $CeO_{2-x}$ nanorods (including the nanocubes) exhibited characteristic peaks corresponding to the crystal planes of (111), (200), (220) and (311) (Fig. 2A), which were indicative of pure cubic phases and in agreement with the reported fluorite structure of CeO2 crystals (JCPDS 34-0394). Higher concentrations of NaOH led to greater crystallinity of the $CeO_{2-x}$ nanorods.[25] The bulk crystallinity of the $CeO_{2-x}$ nanoparticles (hence non-porous crystalline internal structure) was further corroborated by TEM results (Figure 1A inset). Note that Scanning Electron Microscopy (SEM) were not used here because it provided a resolution of ~10 nm (limited by the width

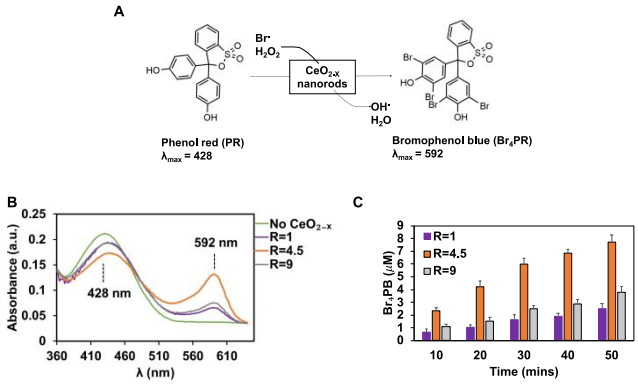


**Fig. 3. HPO-like catalytic activity of $CeO_{2-x}$ nanorods/nanocubes.** (A) Scheme of the oxidative bromination of PR to $Br_4PR$. (B) UV-vis spectra collected during the PR bromination assay for $CeO_{2-x}$ nanorods/nanocubes. The spectra were collected at the end of 10 minutes of reaction time, with the $H_2O_2$ concentration of 10 μM and the $Br^-$ concentration of 10 mM. (C) The amount of $Br_4PB$ generated over time using the $CeO_{2-x}$ nanorods/nanocubes with different R values. Data are mean ± SD (n = 3).



Please do not ad

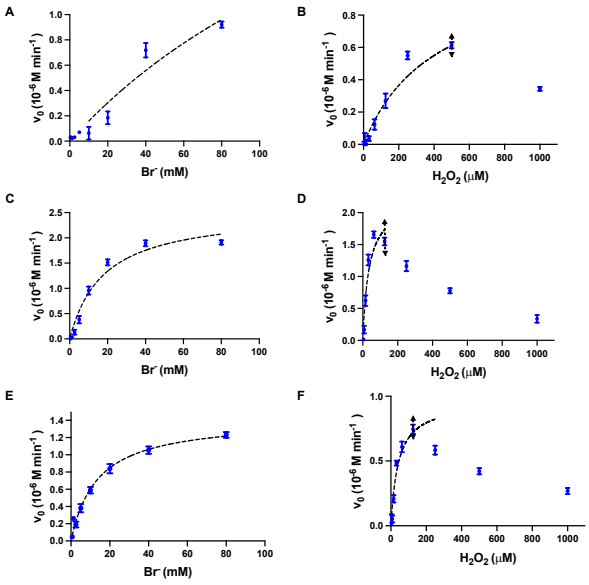


**Fig. 4. Kinetics of bromination as a function of the substrate concentrations for $CeO_{2-x}$ nanorods R=1 (A, B), R=4.5 (C, D) and R=9 (E, F).** The values (blue dots) were fitted to the Michaelis-Menten equation (black dashed line). The concentration of $CeO_{2-x}$ nanorods was 0.04 mg/mL (in 5 mM MES buffer with 25 μM Phenol red). To obtain the Michaelis-Menten constant ($K_m$) for Br$^-$, the concentration of $H_2O_2$ were kept constant at 250 μM. To obtain the $K_m$ for $H_2O_2$, the concentration of Br$^-$ were kept constant at 10 mM. The fitting range for $H_2O_2$ is illustrated by the black double arrows.

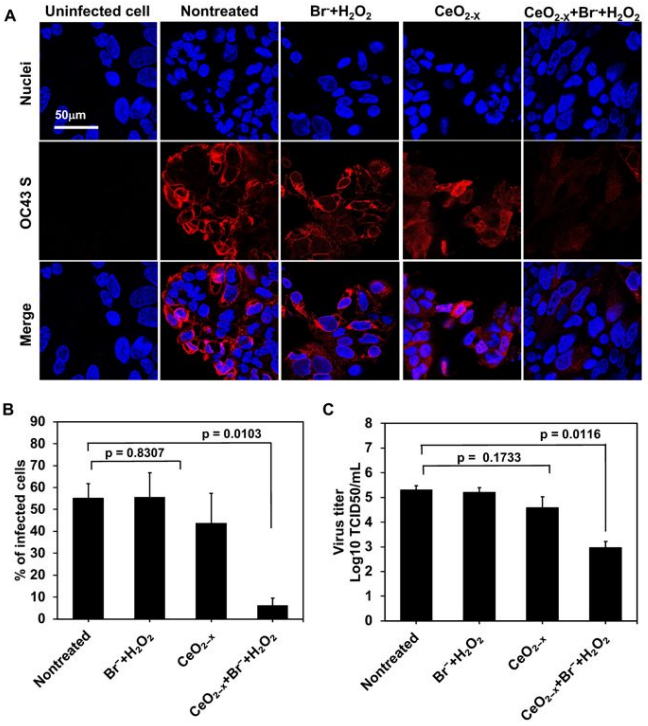


**Fig. 5 Deactivation of coronavirus OC43 using the $CeO_{2-x}$ nanorods (with R=4.5).** (A) Immunofluorescence imaging of the HCT-8 cells infected by OC43 (with the MOI of 0.5) at 48 hours post infection. OC43 S indicates the spike protein of OC43 (red); nuclei of the HCT-8 cells were stained by Hoechst 33258 (blue). (B) The amount of infected cells, i.e., OC43 S-positive cells, quantified using the immunofluorescence images. Data are mean ± SD (n = 5). (C) Reduction of the virus titer by the formulation containing 0.04 mg/mL $CeO_{2-x}$, 1 mM Br$^-$, and 10 μM $H_2O_2$, quantified by the TCID50 assay with the tissue culture infection dose of 50%. Data are mean ± SD (n = 3).

of the excitation electron beam), which was insufficient for resolving the internal structure of the $CeO_{2-x}$ nanoparticles.

High-resolution X-ray photoelectron spectroscopy (XPS) was performed on Ce(3d) to quantify the Ce(III) content of the as-synthesized $CeO_{2-x}$ nanorods. Binding energy of Ce(3d) fell in the range of 930-875 eV (Fig. 2B to 2D, Table S2), based on which, content of Ce(III) in the $CeO_{2-x}$ nanorods was quantified via peak deconvolution with respect to the $3d_{5/2}$ and $3d_{3/2}$ transitions. The $CeO_{2-x}$ nanorods with R=4.5 demonstrated the highest Ce(III) content, i.e., 47.1% of all Ce species was Ce(III). The $CeO_{2-x}$ nanocubes (R=1) and the $CeO_{2-x}$ nanorods with R=9 demonstrated a comparable Ce(III) content of ~33%. The corresponding survey spectra confirmed that Ce and O were the main elements and the relative atomic ratio, i.e., O/Ce, fell in the range of 6.5 to 7.7. It was greater than the theoretical value (which should be <2 based on the stoichiometry) due to adventitious oxygen, consistent with previous reports (Fig. S3).[21] Based on these XPS results, we predicted that the $CeO_{2-x}$ nanorods with R=4.5 would exhibit the highest HPO-like catalytic activities, which was tested as described below. The HPO-like activities of $CeO_{2-x}$ nanorods have been shown to positively correlate with the content of the reactive surface sites of Ce(III).[21]

The HPO-like catalytic activities of $CeO_{2-x}$ nanorods/nanocubes were characterized systematically using the phenol red (PR) bromination assay.[21] The HPO-like catalytic activity was indicated by a shift of UV-vis absorption from that of PR ( λmax = 428 nm) to that of bromophenol blue ($Br_4$PR, 3′ ,3″ ,5′ ,5″ -tetrabromophenolsulfonphthalein, λmax = 592 nm) (Fig. 3A), corresponding to the bromination of PR. Using UV-vis spectrophotometer and a 25 mM aqueous solution of PR, the aforementioned absorption shift was observed for all nanorods/nanocubes (R=1, 4.5 and 9, dissolved at the concentration of 0.04 mg/mL with 10 mM $H_2O_2$ and 10 mM Br$^-$ ) (Fig. 3B). In contrast, no bromination occurred in the absence of the $CeO_{2-x}$ nanorods, or Br$^-$, or $H_2O_2$ (Fig. S2). The amount of $Br_4$PR generated over time was quantified for all $CeO_{2-x}$ nanorods/nanocubes (Fig. 3C), which indicated that the $CeO_{2-x}$ nanorods with R=4.5 had the highest HPO-like catalytic activity, which was 4 times that of $CeO_{2-x}$ nanocubes and double that of $CeO_{2-x}$ nanorods with R=9 (with 0.04 mg/mL $CeO_{2-x}$, 10 mM $H_2O_2$ and 10 mM Br$^-$). The catalytic activities of the $CeO_{2-x}$ nanorods/nanocubes were characterized in detail with respect to their aspect ratios, by quantifying the kinetic parameters, such as the Michaelis-Menten constants ($K_m$) for Br$^-$ and $H_2O_2$, respectively, and the maximum reaction, $V_{max}$. The kinetic parameters were obtained by varying the concentrations of one substrate (e.g., that of Br$^-$ in the range of 0-80 mM or that of $H_2O_2$ in the range of 0-1000 mM) while keeping the concentrations of the remaining components constant (i.e., 0.04 mg/mL $CeO_{2-x}$ and 25 mM PR). The $K_m$ and $V_{max}$ values were determined by Lineweaver-Burk linearization (Fig. 4), with the kinetics data shown in Table S3.[21] The $CeO_{2-x}$ nanorods with R=4.5 demonstrated slightly greater $K_m$ value with respect to Br$^-$ (i.e., 17.9 mM) than that of the $CeO_{2-x}$ nanorods with R=9 (i.e., 13.5

mM), whereas the $K_m$ value with respect to $H_2O_2$ showed the opposite trend (i.e., 35 mM for the $CeO_{2-x}$ nanorods with R=4.5 and 41.8 mM for the $CeO_{2-x}$ nanorods with R=9). The $CeO_{2-x}$ nanocubes (i.e., R=1) demonstrated much higher $K_m$ values with respect to $Br^-$ (i.e., 206.9 mM) and $H_2O_2$ (476.8 mM) compared to those of the $CeO_{2-x}$ nanorods. While a mild substrate-inhibitory effect was observed at $H_2O_2$ concentrations greater than 125 mM and 500 mM for the $CeO_{2-x}$ nanorods and nanocubes respectively, it was consistent with the previous reports on nanoparticles of vanadium pentoxide[10] and cerium oxides,[21] although the mechanism remained elusive.

These $K_m$ values revealed that the $CeO_{2-x}$ nanorods (i.e., with R=4.5 and R=9) had similar substrate-binding affinities, which held true for both $H_2O_2$ and $Br^-$, whereas the $CeO_{2-x}$ nanocubes (i.e., R=1) had much lower substate-binding affinity. Even though the $CeO_{2-x}$ nanocubes (R=1) have the highest $V_{max}$, its lowest substrate-binding affinity reduced the HOBr-generating capacity in the presence of low substrate concentrations (e.g., 10 mM used in the following anti-virus test[10]). Based on these kinetics results, we chose $CeO_{2-x}$ nanorods with R=4.5, which demonstrated high rate of HOBr generation and strong substrate-binding affinity, to demonstrate the virucidal effect of $CeO_{2-x}$ nanoparticles.

The virucidal effect of the $CeO_{2-x}$ nanorods (with R=4.5) was assessed using HCoV-OC43 (OC43), one of the seven human coronaviruses discovered to date.[27] It is also considered the most common human coronavirus worldwide, with the highest rate of incidence during winter and spring months.[27] To assess the inactivation effects of the $CeO_{2-x}$ nanorods on viral infections, suspensions of OC43 were incubated with the formulation that contains 0.04 mg/mL $CeO_{2-x}$, 1 mM $Br^-$, and 10 mM $H_2O_2$, or control groups that were nontreated, or treated with the $CeO_{2-x}$ nanorods alone, or treated with 1 mM $Br^-$ and 10 mM $H_2O_2$. All formulations were incubated with OC43 suspensions for 15 minutes. The incubated virus suspensions were subsequently collected and used to infect HCT-8 host cells (via co-incubation for 2 hours, followed by removal of unattached virus particles and incubation of the infected HCT-8 cells for 48 hours) to assess the infection activities of the viruses that were nontreated or treated using the three aforementioned formulations. The OC43 virus achieved an infection rate of 55.3% ± 6.6% in the HCT-8 cells at the multiplicity (MOI) of 0.5 at 48 hours post infection (Fig. 5A and 5B). That infection rate was greatly reduced to 6.1% ± 3.4% for the virus suspensions that were incubated with the formulation (i.e., 0.04 mg/mL $CeO_{2-x}$ nanorods, 10 mM $H_2O_2$, and 1 mM $Br^-$) for merely 15 minutes, indicating strong antiviral effects of the catalytic system. The infection rate was mildly reduced to 43.7% ± 13.6% for virus suspensions treated with the $CeO_{2-x}$ nanorods alone and was not affected by the treatment with $Br^-$ and $H_2O_2$, i.e., 55.7 ± 11.0%. The slight antiviral effect of the $CeO_{2-x}$ nanorods alone could be attributed to a mechanism reported previously,[28] where adhesion of virus particles onto the

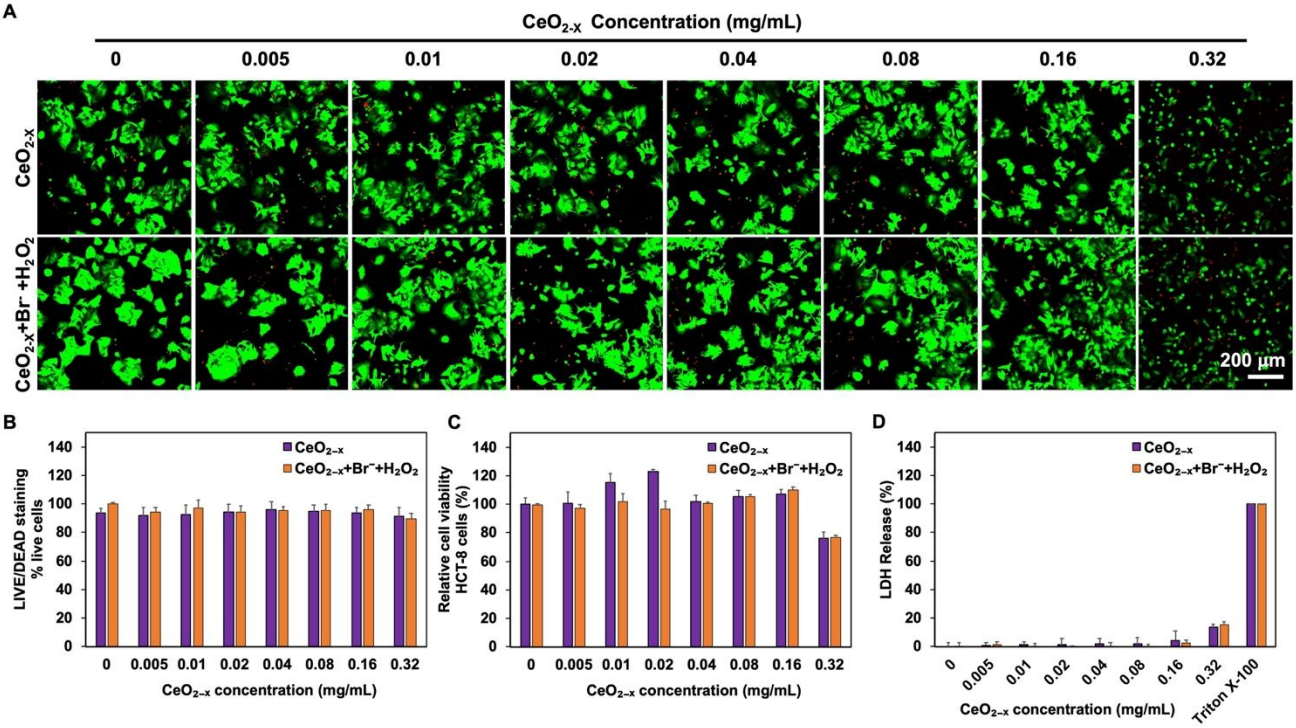


**Fig. 6 Cytotoxicity of the $CeO_{2-x}$ nanorods and formulations.** (A) LIVE/DEAD staining images. HCT-8 cells were treated with the nanorods or formulations at various concentrations for 72 hours. The concentrations of $H_2O_2$ and $Br^-$ were kept at 10 μM and 1 mM respectively for all groups, while the concentration of $CeO_{2-x}$ nanorods was varied systematically in the range of 0-0.32 mg/mL. Green color, viable cell; red color, dead cell. (B) HCT-8 cell survival rate (% live cells), obtained by counting the live and dead cells in panel. The percentage of live cells were calculated as [live cells/(live cells + dead cells) × 100%], where cell counts were obtained using ImageJ. Data are mean ± SD. (n = 5). (C) Viability of the treated HCT-8 cells, quantified via CCK-8 kit after 72 hours of incubation with the $CeO_{2-x}$ nanorods or formulations. The concentrations of $H_2O_2$ and $Br^-$ were kept at 10 μM and 1 mM respectively for all groups, while the concentration of $CeO_{2-x}$ nanorods was varied systematically in the range of 0-0.32 mg/mL. Data are mean ± SD. (n = 5). (D) LDH release from the HCT-8 cells treated with the $CeO_{2-x}$ nanorods or formulations. Data are mean ± SD. (n = 5).


This journal is © The Royal Society of Chemistry 20xx

nanorods during the 15-minute incubation step reduced the active virus number that could infecting the host cells. Although $CeO_{2-x}$ nanorods have been reported to produce several classes of ROS (e.g., HOBr, hydroxyl radials, and superoxide anions), our results confirmed that the $CeO_{2-x}$ nanorods alone likely did not produce sufficient ROS to achieve deactivation of viruses. Virulence of the OC43 virus was assessed by the fifty-percent tissue culture infective dose (TCID50) assay, where virus titers were quantified after incubation with the aforementioned formulations for 15 minutes. The average viral titer in the nontreated OC43 suspension corresponded to a log (TCID50/mL) value of 5.3, which was reduced to 2.9 after incubating viral suspensions with the formulation (i.e., 0.04 mg/mL $CeO_{2-x}$ nanorods, 10 mM $H_2O_2$, and 1 mM $Br^-$) for merely 15 minutes (Fig. 5C). It corresponded to a 99.5% reduction of the virulence of OC43, indicating strong antiviral efficacies of the formulation containing $CeO_{2-x}$ nanorods, $Br^-$, and $H_2O_2$. That excellent antiviral efficacy also hints at the resistance to protein adsorption of the $CeO_{2-x}$ nanorods, as the protein concentration in the OC43 culture was ~ 0.2 mg/mL. That resistance to protein adhesion could be attributed to the negative surface charge of the $CeO_{2-x}$ nanorods (Table S1), corresponding to a Zeta potential of ~-14mV, which has been reported to lead to little or no protein adsorption.[29]

To evaluate the cytotoxicity of the formulations and the $CeO_{2-x}$ nanorods, HCT-8 cells were incubated with formulations of various $CeO_{2-x}$ concentrations for 72 hours, followed by viability assessment using the LIVE/DEAD staining, CCK-8 assay, and lactate dehydrogenase (LDH) release assay (Fig. 6). No toxicity to the HCT-8 cells was observed in LIVD/DEAD staining (Fig. 6A and 5B) when the concentration of $CeO_{2-x}$ nanoparticles was kept at or below 0.16 mg/mL, where a majority of the HCT-8 cells remained alive (as indicated by the green color). Additional CCK-8 assays were performed following an incubation period of 72 hours (Fig. 6C). The formulations with the $CeO_{2-x}$ concentrations below 0.16 mg/mL retained the cell viability completely. Mild cytotoxicity was only observed at the highest $CeO_{2-x}$ concentration (i.e., 0.32 mg/mL) with a cell viability of 76.1 ± 4.6%.

Furthermore, we performed lactate dehydrogenase (LDH) release assays to further assess the membrane integrity of the treated HCT-8 cells (Fig. 6D). Again, the LDH assays indicated minimal cytotoxicity when the concentration of $CeO_{2-x}$ was varied between 0 and 0.16 mg/mL; whereas the concentration of 0.32 mg/mL led to 13.4 ± 2.0% LDH release compared to the non-treated HCT-8 cells, consistence with the LIVE/DEAD staining and CCK-8 results. Similarly, the formulation containing 10 μM $H_2O_2$, 1 mM $Br^-$, and 0.32 mg/mL $CeO_{2-x}$ led to 15.1 ± 2.3% LDH release, comparable to that of $CeO_{2-x}$ alone. The mild cytotoxicity at the concentration of 0.32 mg/mL was likely a result of the precipitation of $CeO_{2-x}$ that formed at this concentration, which could cause cell damage via known interactions.[30] Overall, these results indicated excellent biocompatibility of the nanorod formulations.

## Discussion

Here, we successfully synthesized $CeO_{2-x}$ nanorods with different aspect ratios. The HPO-like activity of the $CeO_{2-x}$ nanorods was studied extensively using the phenol red bromination assay. Our result demonstrated that $CeO_{2-x}$ nanorod with the length-to-diameter ratio of 4.5 led to the highest HPO-like activity, likely a result of the high content of Ce(III) surface active sites. The two stable oxidation states of Cerium, i.e., Ce(III), with a partially occupied *f* orbital, and Ce(IV), with an empty *f* orbital, collectively enable the HPO-like activities. As such, the value of "x" in $CeO_{2-x}$ could range between 0 and 0.5, with a greater number of oxygen vacancies in the $CeO_2$ lattice as x increases. The oxygen vacancies are known to act as binding sites for catalytically active species, and thus lead to greater catalytic activities. In general, $CeO_{2-x}$ are known to have non-stoichiometric anion deficiencies, and the value of x ($0 < x < 0.5$) depends on the synthesis and processing conditions. In our work, $CeO_{2-x}$ nanorod (R=4.5) demonstrated a Ce(III) content of 47.1%, corresponding to a molecular formula of $CeO_{1.765}$ (with an x value of 0.235). The greater catalytic and antiviral activities for $CeO_{2-x}$ nanorod (R=4.5) can thus be explained by its greater number of oxygen vacancies (e.g., the $CeO_{2-x}$ nanorod (R=9) has a Ce(III) content of 33.2%, corresponding to an x value of 0.145). A formulation containing 0.04 mg/mL $CeO_{2-x}$ nanorod (R=4.5), 10 mM $H_2O_2$, and 1 mM $Br^-$ reduced the virulence of a human coronavirus, HCoV-OC43, by 99.5% without causing cytotoxicity.

Our results illustrated that the $CeO_{2-x}$ nanorods were able to convert hydrogen peroxide into hypobromous acid, and the catalytic reactivity of the as-synthesized $CeO_{2-x}$ nanorods was comparable to those reported in the literature for a range of HPOs.[21] As hypohalous acids often emerge as the first line of defense in the war against SARS-CoV-2 due to its powerful oxidizing effect against all essential building blocks of a virus particle, including protein, DNA and lipid.[32] The antiviral hypobromous acid is also known to be biocompatible as hypohalous acids has been approved by the U.S. Food and Drug Administration (FDA) as an active ingredient for eyedrops.[33, 34]The antiviral effects of hypobromous acid that the catalytic $CeO_{2-x}$ nanorods demonstrated active virucidal efficacy.

Once applied in vivo, the catalytic reactions are unlikely sustained by the naturally occurring bromide in the human body due to its low abundance. For example, the concentration of bromide is about 0.01mM in lung and liver,[35] and about 0.03-0.14 mM in blood.[36, 37]; whereas the range of concentrations commonly used to demonstrate HPOs-like activities is 1.25 mM to 80 mM. Nevertheless, we believe this low concentration of baseline bromide in the human body could be advantageous for avoiding undesirable side reactions and improving the biocompatibility of this therapeutic system. For example, high concentrations of bromide could be co-delivered along with the $CeO_{2-x}$ nanorods to the desired anatomic location to achieve high efficacy using established delivery vehicles.[38]

Future work will focus on testing the antiviral efficacy of the $CeO_{2-x}$ nanorods in vivo and unravelling its pharmacokinetics (for systemic or topical applications). Furthermore, we believe the materials reported here could be applied in settings much beyond medicine, for example, as a coating material for public

facilities to prevent fomite transmission. To the best of our knowledge, this was the first report on the virucidal activities of $CeO_{2-x}$ nanorods, which pointed to their applications as antiviral materials and/or therapeutics. For example, the nanorods could be delivered locally to activated macrophages, enabling the conversion of the $H_2O_2$ (generated by macrophages) to hypohalous acids and thus boosting the overall antimicrobial effects. Extensive prior studies have hinted at the tolerance of macrophages towards $CeO_{2-x}$ nanorods, increasing the likelihood of success for such a design, which will be an important focus of our future study.

This work was supported by the Department of the Navy, Office of Naval Research (ONR award N00014- 20-1-2418), National Institutes of Health, National Institute on Deafness and Other Communication Disorders (NIHDC016644).

## Author Contributions

JL and XM contributed equally to this work.
JL and RY conceived the idea and designed the experiments. JL and MS synthesized the nanoparticles. JL, XM, PC and NMR conducted the experiment and data analysis. RY, GWR supervised the study. The manuscript was prepared by JL, XM and RY.

## Conflicts of interest

Authors state that there are no conflicts to declare.

## Notes and references

1. D. M. Morens and A. S. Fauci, *Cell*, 2020, **182**, 1077-1092.
2. D. E. Bloom and D. Cadarette, *Front Immunol*, 2019, **10**, 549-549.
3. L. A. Reperant and A. D. M. E. Osterhaus, *Vaccine*, 2017, **35**, 4470-4474.
4. E. De Clercq and G. Li, *Clin. Microbiol. Rev.*, 2016, **29**, 695-747.
5. K. Lesser and G. R. Whittaker, *Public Health*, 2021, DOI: 10.1016/j.puhe.2021.02.002.
6. S. Ojosnegros and N. Beerenwinkel, *Immunome Res.*, 2010, **6 Suppl 2**, S5-S5.
7. M. S. Block and B. G. Rowan, *J. Oral Maxillofac. Surg.*, 2020, **78**, 1461-1466.
8. D. W. Stroman, K. Mintun, A. B. Epstein, C. M. Brimer, C. R. Patel, J. D. Branch and K. Najafi-Tagol, *Clin. Ophthalmol.*, 2017, **11**, 707-714.
9. H. Hakim, C. Thammakarn, A. Suguro, Y. Ishida, A. Kawamura, M. Tamura, K. Satoh, M. Tsujimura, T. Hasegawa and K. Takehara, *J. Vet. Med. Sci.*, 2015, **77**, 211-215.
10. F. Natalio, R. Andre, A. F. Hartog, B. Stoll, K. P. Jochum, R. Wever and W. Tremel, *Nat. Nanotechnol.*, 2012, **7**, 530-535.
11. M. E. Belding, S. J. Klebanoff and C. G. Ray, *Science*, 1970, **167**, 195-196.
12. A. Ulfig and L. I. Leichert, *Cell. Mol. Life Sci.*, 2021, **78**, 385-414.
13. K. Herget, H. Frerichs, F. Pfitzner, M. N. Tahir and W. Tremel, *Adv. Mater.*, 2018, **30**, 1707073.
14. R. Zhang, X. Yan and K. Fan, *Acc. Mater. Res.*, 2021, **2**, 534-547.
15. A. A. Akande, A. G. J. Machatine, B. Masina, G. Chimowa, B. Matsoso, K. Roro, M. M. Duvenhage, H. Swart, J. Bandyopadhyay, S. S. Ray and B. W. Mwakikunga, *Journal of Physics D-Applied Physics*, 2018, **51**.
16. J. Wu, X. Wang, Q. Wang, Z. Lou, S. Li, Y. Zhu, L. Qin and H. Wei, *Chem. Soc. Rev.*, 2019, **48**, 1004-1076.
17. E. G. Heckert, A. S. Karakoti, S. Seal and W. T. Self, *Biomaterials*, 2008, **29**, 2705-2709.
18. T. Pirmohamed, J. M. Dowding, S. Singh, B. Wasserman, E. Heckert, A. S. Karakoti, J. E. King, S. Seal and W. T. Self, *Chem. Commun. (Camb.)*, 2010, **46**, 2736-2738.
19. X. Zhou, M. You, F. Wang, Z. Wang, X. Gao, C. Jing, J. Liu, M. Guo, J. Li, A. Luo, H. Liu, Z. Liu and C. Chen, *Adv. Mater.*, 2021, **33**, 2100556.
20. B. L. Zhang, H. Y. Yu, J. Q. Wang, W. B. Wang, Q. Y. Zhang and H. P. Zhang, *J. Am. Ceram. Soc.*, 2019, **102**, 2218-2227.
21. K. Herget, P. Hubach, S. Pusch, P. Deglmann, H. Götz, T. E. Gorelik, I. y. A. Gural'skiy, F. Pfitzner, T. Link, S. Schenk, M. Panthöfer, V. Ksenofontov, U. Kolb, T. Opatz, R. André and W. Tremel, *Adv. Mater.*, 2017, **29**, 1603823.
22. H. Frerichs, E. Pütz, F. Pfitzner, T. Reich, A. Gazanis, M. Panthöfer, J. Hartmann, O. Jegel, R. Heermann and W. Tremel, *Nanoscale*, 2020, **12**, 21344-21358.
23. Q. Weng, H. Sun, C. Fang, F. Xia, H. Liao, J. Lee, J. Wang, A. Xie, J. Ren, X. Guo, F. Li, B. Yang and D. Ling, *Nat. Commun.*, 2021, **12**, 1436.
24. M. Das, S. Patil, N. Bhargava, J. F. Kang, L. M. Riedel, S. Seal and J. J. Hickman, *Biomaterials*, 2007, **28**, 1918-1925.
25. X. He, F. Tian, J. Chang, X. Bai, C. Yuan, C. Wang and A. Neville, *ACS Sustain. Chem. Eng.*, 2020, **8**, 6744-6752.
26. M. Hirano and E. Kato, *J. Am. Ceram. Soc.*, 1999, **82**, 786-788.
27. S. Park, Y. Lee, I. C. Michelow and Y. J. Choe, *Open Forum Infect. Dis.*, 2020, **7**.
28. B. De Gusseme, G. Du Laing, T. Hennebel, P. Renard, D. Chidambaram, J. P. Fitts, E. Bruneel, I. Van Driessche, K. Verbeken, N. Boon and W. Verstraete, *Environ. Sci. Technol.*, 2010, **44**, 6350-6356.
29. S. Patil, A. Sandberg, E. Heckert, W. Self and S. Seal, *Biomaterials*, 2007, **28**, 4600-4607.
30. A. Sukhanova, S. Bozrova, P. Sokolov, M. Berestovoy, A. Karaulov and I. Nabiev, *Nanoscale Res. Lett.*, 2018, **13**, 44-44.
31. R. K. Hailstone, A. G. DiFrancesco, J. G. Leong, T. D. Allston and K. J. Reed, *J. Phys. Chem. C*, 2009, **113**, 15155-15159.
32. C. L. Hawkins, D. I. Pattison and M. J. Davies, *Amino Acids*, 2003, **25**, 259-274.
33. S. Sakarya, N. Gunay, M. Karakulak, B. Ozturk and B. Ertugrul, *Wounds*, 2014, **26**, 342-350.
34. M. M. Kiamco, H. M. Zmuda, A. Mohamed, D. R. Call, Y. S. Raval, R. Patel and H. Beyenal, *Scientific Reports*, 2019, **9**, 2683.
35. M. Kohlmeier, in *Nutrient Metabolism (Second Edition)*, ed. M. Kohlmeier, Academic Press, San Diego, 2015, DOI: https://doi.org/10.1016/B978-0-12-387784-0.00011-0, pp. 673-807.
36. H. A. Olszowy, J. Rossiter, J. Hegarty and P. Geoghegan, *J. Anal. Toxicol.*, 1998, **22**, 225-230.
37. T. Yamauchi, D. Nagashima, S. Okubo, A. Kokaze and Y. Yamano, *J. Occup. Health*, 2021, **63**, e12274.
38. R. Yang, V. Sabharwal, O. S. Okonkwo, N. Shlykova, R. Tong, L. Y. Lin, W. Wang, S. Guo, J. J. Rosowski, S. I. Pelton and D. S. Kohane, *Sci. Transl. Med.*, 2016, **8**.

 This journal is © The Royal Society of Chemistry 20xx